SINUSOIDAL LEADING EDGE FOR PASSIVE FLOW CONTROL IN VAWT

L. Tieghi[1], G. Delibra[2], G. Gaeta[3], A. Corsini[2]*

[1] Department of Civil, Environmental and Mechanical Engineering, Via Mesiano 77, 38123, Trento, Italy
[2] Department of Mechanical and Aerospace Engineering, Via Eudossiana 18, 00184, Rome, Italy
3Technip Energies Italy S.P.A., Viale Castello della Magliana, 00148, Rome, Italy

Abstract

Vertical Axis Wind Turbines (VAWTs) are a promising technology for renewable energy communities, and also receiving increasing interest for offshore applications due to their potential cost advantages over horizontal-axis rotors. In this study, we investigate a modification to the rotor blades, inspired by patterns observed in the pectoral fins of humpback whales, aiming at increasing the performance in terms of efficiency. To this aim, the blades of a reference Darrieus wind turbine characterized by a NACA0015 airfoil with a chord length c = 0.4 m and a zero-pitch angle were fitted with a sinusoidal leading edge, characterized by an amplitude of 0.06c and a wavelength of 0.5c. The analysis was carried out using OpenFOAM-v23, performing a time-dependent simulation based on a sliding interface approach and the PIMPLE solver. The results show that the sinusoidal leading edge can significantly enhance aerodynamic performance during blade stall and post-stall, with a substantial recovery in lift coefficient. However, under a stable angle of incidence, a slight decline in aerodynamic performance is observed. Additionally, the overall efficiency loss of the machine led to increased stress due to the sudden oscillation of the acting forces.

Keywords: vertical axis wind turbines, flow control, sinusoidal leading edge, biomimicry

1 Introduction

The push for renewable energy has led to 255 GW of installed wind energy capacity in Europe, 225 GW onshore and 30 GW offshore. Current European programs have planned the deployment of additional 98 GW of new wind capacity (mostly offshore) to meet the renewable energy targets for 2030 [1]. These investments aim to install large-scale wind farms equipped with state-of-art Horizontal Axis Wind Turbines (HAWTs), with nominal power up to 15 MW. Nevertheless, the concerning increase of operational costs for HAWTs is leading to consideration of possible installation of VAWTs in offshore environments. In addition, their small size and low cut-in velocity allow their installation in local renewable energy communities.

However, despite a long history of VAWTs development, the widespread adaptation of this technology is still limited by several factors. First, the lower aerodynamic efficiency compared to HAWTs, resulting in reduced energy production [2]. Moreover, self-starting and shutdown still pose significant challenges [3]. On the aerodynamic side, the existing configurations of VAWTs lead to detrimental interaction between one blade and the wake released by the previous one, leading to stalled conditions for a significant portion of the rotor revolution.

Several works have investigated passive flow control methods to improve the aerodynamic efficiency of the blades. For example, Mostafa et al. [4] have installed a micro-cylinder in front of the leading edge, that induces a redistribution of pressure on the surface of the profile and keeps the flow attached and delays separation. Zhu et al. [5] have introduced a slotted airfoil, that increases pressure at the leading edge and, for some profiles lead to a delay of stall up to angles of attack of 20°. A different modification to the airfoil shape is proposed by Zamani et al. [6], who tested a J-shaped airfoil which improves the automatic starting of the rotor and the torque and power coefficients. The J-shaped profile retains vorticity in its cup-like form, reducing wake extension, turbulence and noise. Even if technologically still complex to manufacture, VAWTs could also benefit from the adoption of adaptive blades, as shown by Wang et al. [10].

In this paper, we explore the capability of a biomimetic modification to the blades that is inspired to the tubercles on the pectoral fins of humpback whales. These animals exploit the unique shape of their fins to maneuver and execute sharp turns while chasing prey. Similarly, the leading edge of the VAWT blades is modified applying a sinusoidal pattern, while retaining the original mean value for the profile chord length. The modified leading-edge induces counter-rotating vortical structures that delay boundary layer separation and lead to an increase in stall margin.

This solution has been previously proved effective in low-speed axial fans to delay separation and to increase the stable operational range of the fan [8]. The modified fans also exhibit enhanced efficiency in presence of distorted inflow conditions, as shown by Tieghi et al. in [9]. However, their application to crossflow turbomachinery and VAWT is scarce. Wang et al. [10] explored the effects of serrations on the leading edge through numerical simulations, varying the sinusoidal geometry, and demonstrated that the turbine with serrated edges showed increased power output at low TSRs, as well as increased torque and lift when the sinusoidal amplitude was small. The findings of this study were corroborated by Wei et al. [11] in their research on hydrodynamic turbines at low Reynolds numbers, confirming that these results are amplified in such conditions. Johari et al. [12] experimentally examined the effects of sinusoidal protuberances on the leading edge in a series of hydrodynamic tunnel tests. Similar results are reported for the trailing edge by Lin et al. [13]. Longhuan et al. [14] experimentally evaluated the self-starting properties of a H-Darrieus turbine, observing an improvement in the case of properly designed tubercles. In [15], long-wavelength protuberances increased the turbine power production by 6.28%. The background mechanism that justifies the performance change was found in the variation of surface pressure coefficient that led to the generation of stall vortices closer to the leading edge of the blades.

In this work, leading edge tubercles are fitted to the blades of a Darreius VAWT, and numerically simulated with unsteady computations. Results are compared at TSR = 1.8 with the baseline geometry to characterize the effects of the modification on the blade aerodynamic properties.

2 VAWT MODEL

The model hereby considered is a three-bladed reference Darreius VAWT. The turbine features a rotor diameter of 2.5 m, a blade height of 3 m and a design TSR of 1.6. The main characteristics are summarized in Table 1. The baseline blades are built with NACA0015 profiles, with a chord length of c=0.4 m. Further details on the turbine are reported in [16]. The NACA profile (hereby denoted as *baseline*) has been modified to include a sinusoidal leading edge (LE) characterized by an amplitude A=0.06c and a wavelength λ=0.5c. The selection of the two parameters is based on the systematic review and design guidelines that are reported in [9].

Table 1 - Characteristics of the VAWT

Diameter	2.5 m
Blade height	3 m
Blade type	Straight NACA 0015
Design TSR	1.6
Design power	3.5 kW
Design rotational speed	12.2 rad/s

The resulting modified turbine blade is shown in Figure 1.

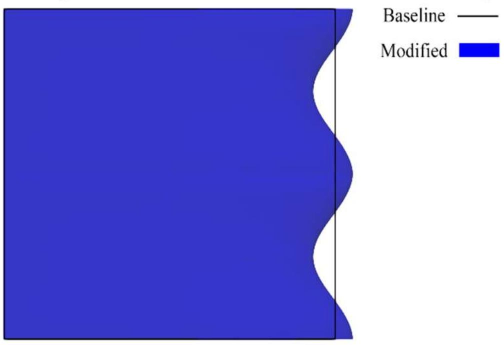

Figure 1 - Scheme of the baseline NACA0015 (solid black line) and modified blade with A = 0.06c and λ = 0.5c (solid surface). Average profile chord c is kept constant with respect to the baseline airfoil.

3 NUMERICAL METHODOLOGY

The turbine operations were simulated with OpenFOAM-v23, with time-dependent simulations.

The computational domain, Figure 13, spans 3D upstream of the turbine shaft and 12D downstream; the lateral overall extension is 8D, following the values reported in [6]. For the baseline geometry a 2D domain in z direction was used, whereas for the modified turbine a full 3D domain was built, simulating only 1/2 of the sinusoid, exploiting symmetry boundary conditions in axial direction, Figure 12.

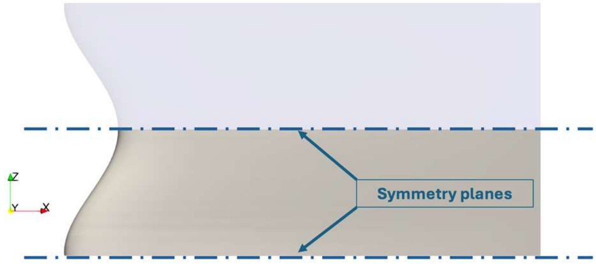

Figure 2 - Axial extent of the 3D domain

The rotating part of the mesh spans 1 meter from the rotor center. The computational grids entails 0.5M and 10M cells for the 2D and 3D cases. Both grids were designed to support low Reynolds computations with a $y^+ < 1$ using hexahedra to discretize the boundary layers on the turbine blades and axis and tetrahedra elsewhere. A-posteriori check of the y^+ value led to an average of 0.71-0.93 for the three blades and peak values ranging from 0.92 to 1.07 at the highest TSR.

The cell distribution in the non-rotating portion of the domain is the same for the two grids. Results of a grid sensitivity study are summarized in Table 2. Grid convergence was assessed against variations of the power coefficient (Cp) with respect to the grid refinement. Results are in line with the grid resolutions of [6], with the most refined mesh (M2) used for the present computations.

Turbulence closure relied on k-w SST turbulence model. The PIMPLE solver was set to 3 inner iterations and a fixed time step $\Delta t = 10^{-5} s$ with Euler 1st order temporal integration scheme. The resulting maximum Courant number oscillated around 0.1.

Boundary conditions were set to uniform velocity equal to the computed wind velocity at the inlet, with turbulence intensity set to 2% and turbulence length-scale equal to 1.5 mm. On the solid walls no-slip boundary conditions were set for velocity and low-Reynolds wall functions were used for turbulent quantities. Outlet of the domain was treated as convective outlet. On the lateral boundaries free-stream conditions were used while in spanwise direction symmetry conditions were imposed on the modified blade simulation. Arbitrary Mesh Interface (AMI) were applied on the sliding interface between rotating and stationary regions.

Table 2 - Grid sensitivity analysis for the 2D computations (TSR 1.6)

ID	Number of cells	Cp
M1	300.000	0.243
M2	540.000	0.261
M3	800.000	0.262

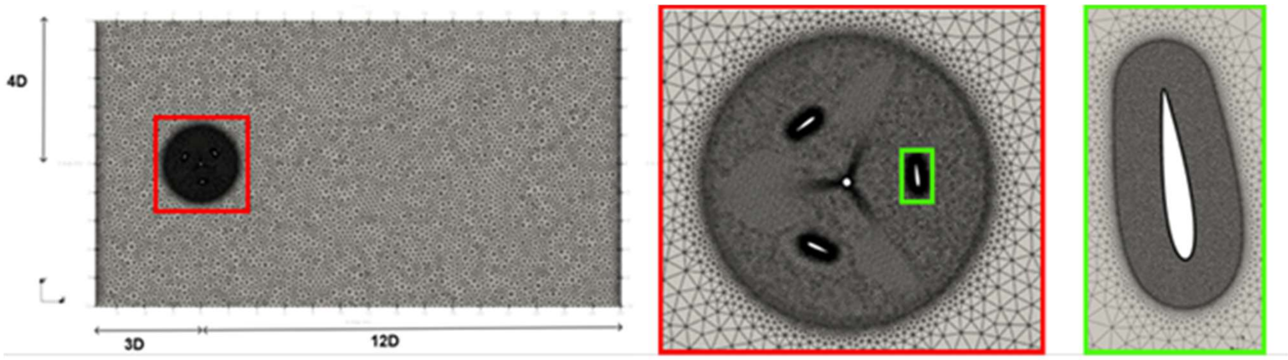

Figure 3 - View of the 2D computational domain and details of the grid.

Computations were run for 10 rotor revolutions to achieve convergent results. Time-averaged data was acquired for the last 10 revolutions. Computations were carried out using 2 x AMD Epyc 9700 CPUs for about 20.000 CPU hours.

4 VALIDATION

Figure 4 shows a comparison in terms of power coefficient $\left(C_p = T\omega / 0.5\rho V^3 bh\right)$ between the computed characteristic curve and the numerical and experimental reference data of [6] and [16]. The current setup shows a fair good agreement with the reference data.

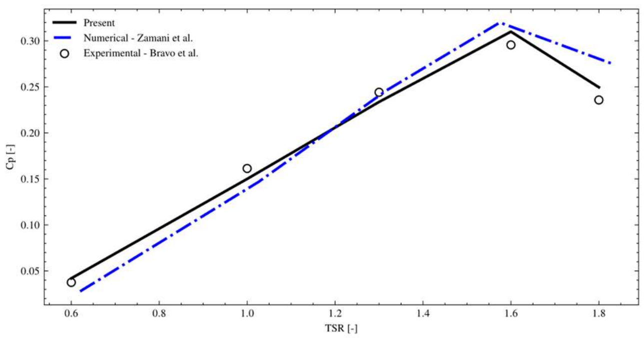

Figure 4 - Predicted power coefficient of the present computations and reference data.

5 RESULTS

The results that are discussed in this section refer to TSR = 1.8, higher than the optimal TSR of 1.6. This choice is justified on one side by the better agreement between numerical setup and experimental (Figure 4) and on the other by the fact that leading edge serrations are more likely improving blade efficiency in suboptimal operating conditions (e.g. post-stall operations).
Leading edge serrations are here responsible of a sensible reduction of -20% in the predicted power coefficient of the turbine, as reported in
Table 3.
Figure 6a shows a breakdown of the fluctuations of the power coefficient for the three blades of the modified turbine.
The sinusoidal leading edge is responsible for a strong fluctuation in the resulting torque, leading to a variation of the

Table 3 - Averaged Cp for different cases

Case	Cp [-]
Bravo et al. (Bravo, 2007)	0.24
Present - baseline	0.25
Present – sinusoidal LE	0.2

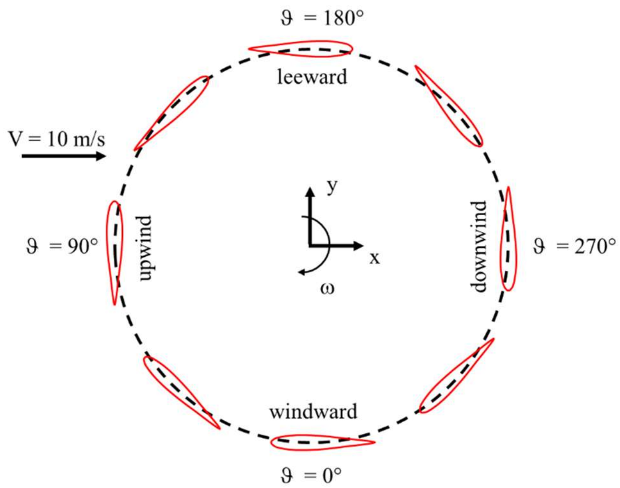

Figure 5 - Scheme of the reference system and blade positioning.

resulting power coefficient. A single blade achieves a peak Cp close to 0.8 at 75°, 195° and 315°, that rapidly decreases to negative values down to -0.2 for the other rotor positions. Notably, in the upwind and downwind position the resulting Cp approximates zero value. The resulting total Cp falls in a similar range of fluctuations, although in an even narrower range of blade positions near the peak Cp positions and a minimum Cp at -0.3.
Figure 6b compares the total and averaged Cp for the two geometries. The leading edge modification induces higher variations in the power coefficient (almost doubled), while achieving an overall reduced power output. A 30° shift between the peaks is observed, presumably induced by the sinusoidal LE.
The large fluctuation of power coefficient of the modified

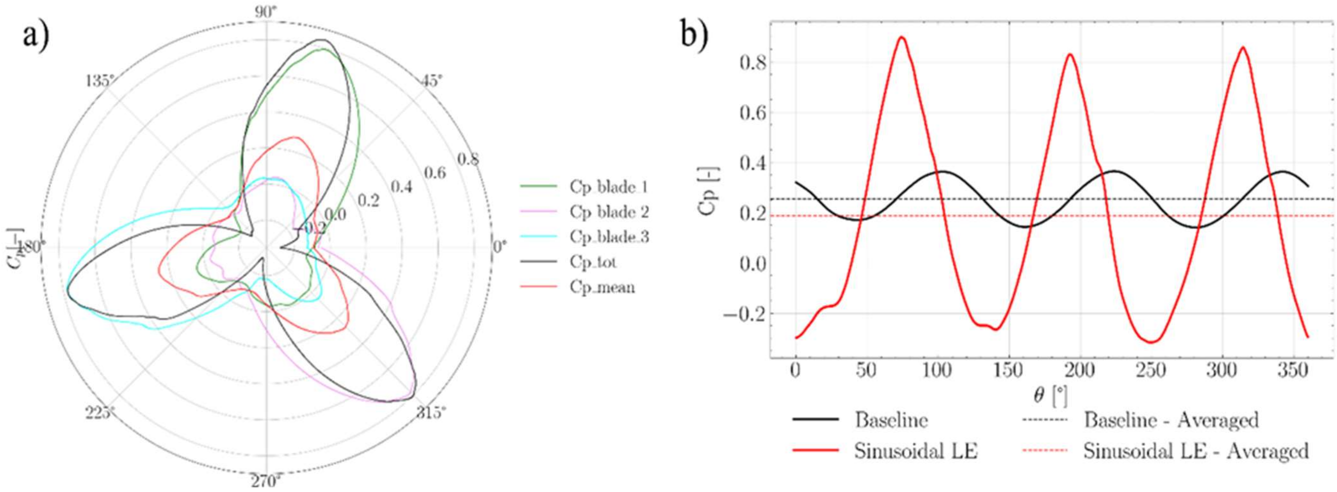

Figure 6 - a) Power coefficient fluctuations of the blades in a rotor revolution and b) comparison with the baseline geometry for a single blade.

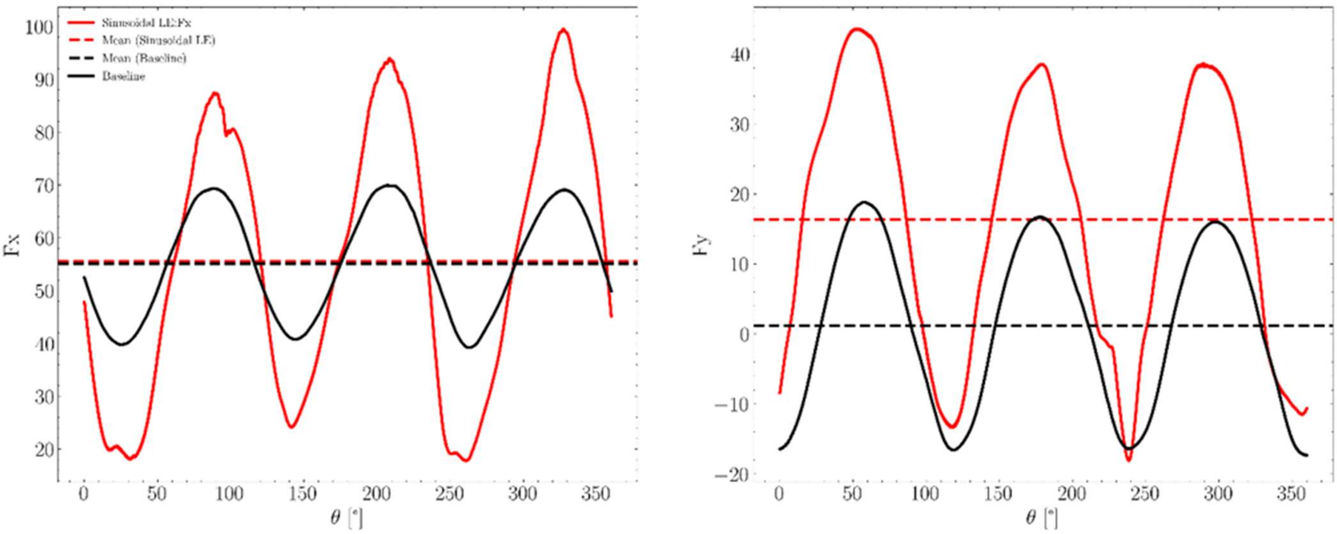

Figure 7 - Streamwise and azimuthal velocities fluctuations over a rotor revolution, comparison between baseline and modified geometries.

blade shown in Figure 6 can be also observed in the streamwise and azimuthal forces Fx and Fy, reported in Figure 7. In the streamwise directions, the two blades exibit a similar resultant of forces, with the modified blade showing a 50% increase in force in the peaks. In the azimuthal direction, the modified blade shows a significant increase in force magnitude in the positive y direction (Figure 5), accordingly with the blade modition direction. The evolution of lift and drag coefficients, shown in Figure 8, explains the behavior of the airfoil. In fact, the major benefits in terms of performance of blade 1 are found (Figure 6) approaching the upwind position, in the range of 45°<θ<90°, where the airfoil is working with increased lift and reduced drag with respect to the baseline geometry (Figure 8). After that, when the blade approaches the leeward direction (90°<θ<180°) the sinusoidal and the baseline airfoils have similar performance. Afterwards, the peak in lift of the sinusoidal airfoil is reduced by 15% with respect to the baseline geometry and this difference remains until the blade reaches again the windward position. Drag coefficient stays the same for both blades up to almost downwind position (θ=270°, Figure 8). After that the sinusoidal blade shows an increase of drag. The combination of the three blades performance led to the results of Figures 6 and 7: where the bumps work in expected conditions there is a significant increase of performance, however, a significant drop occurs in the rest of the revolution.

To explain the drop in performance, Figure 9 shows a time-evolution of velocity contours during the turbine operations. Looking at the snapshot 1), the blade on the upper right is approaching the leeward position. In snapshots 1 and 2 this blade shows a trailing edge separation on the suction surface. After the leeward position (snapshot 3) separation occurs on the pressure surface at the trailing edge and in the following snapshots (4-6) the flow is completely detached, and the airfoil operations are completely compromised. In the final sequence of snapshot 7 to 9, where the airfoil moves from downwind to windward position, the profile regains a proper alignment with the flow.

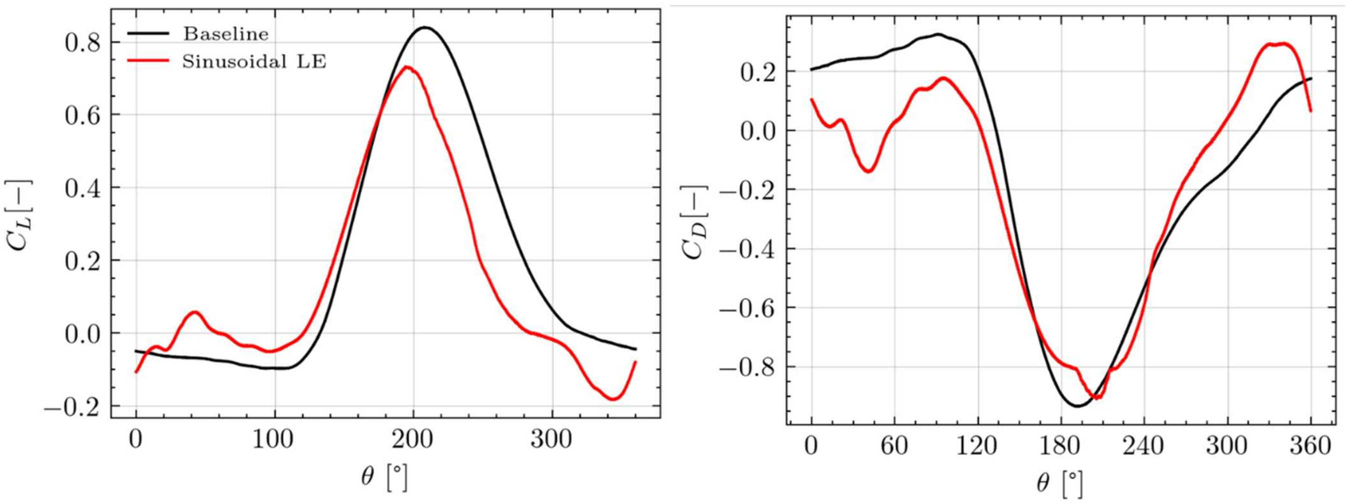

Figure 7 - Lift and drag coefficient variations for a single blade over a rotor revolution, comparison between baseline and modified airfoils.

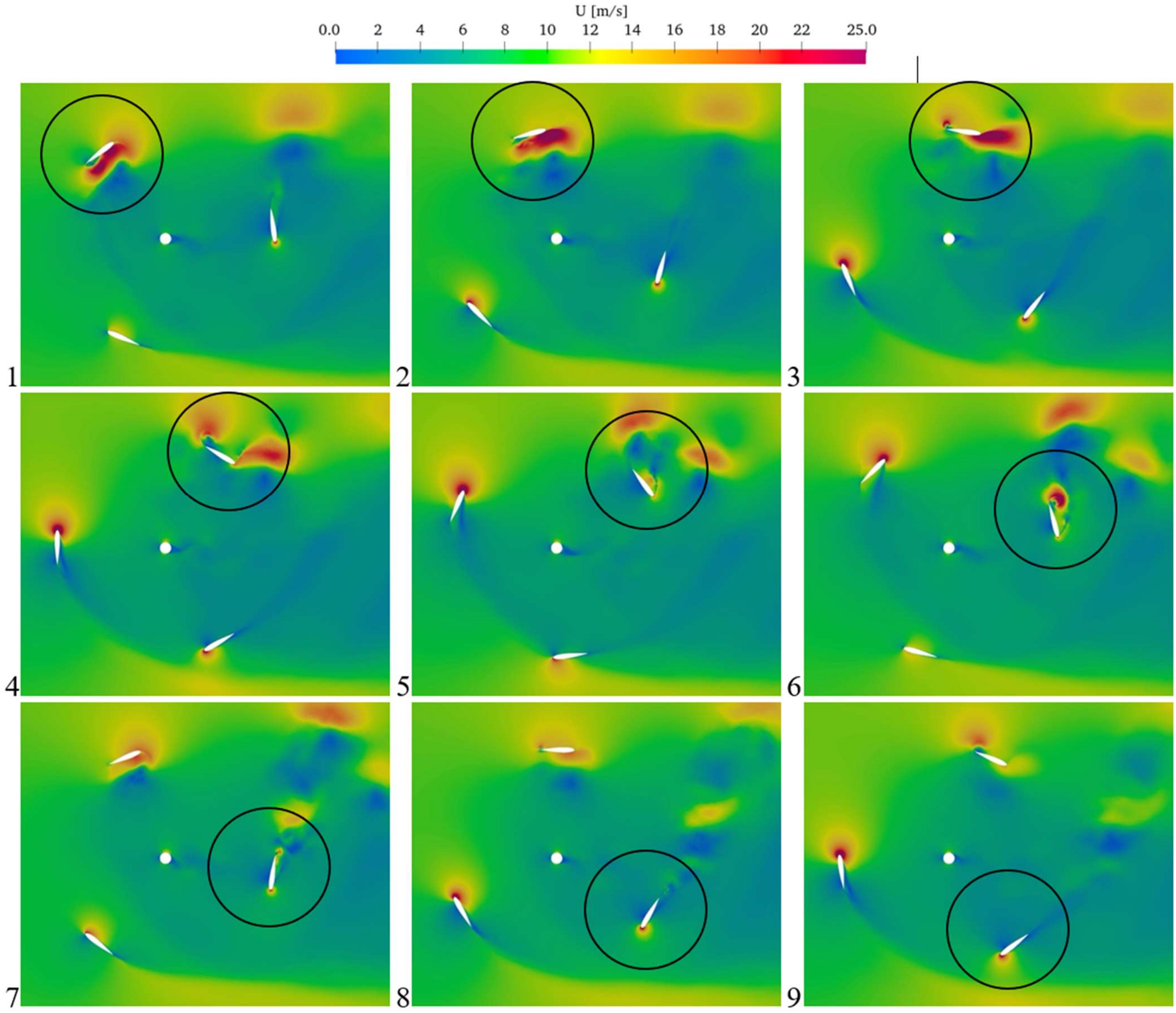

Figure 6 - Time-evolution of velocity contours for the sinusoidal leading edge turbine.

6 CONCLUSIONS

The manuscript investigates the impact of leading-edge tubercles on a reference vertical axis wind turbine. The leading edges of the straight blades were modified to exhibit a sinusoidal pattern with an amplitude of 0.06c and a wavelength of 0.5c. The modified turbine was simulated using unsteady computations in OpenFOAM-23, employing a moving mesh approach. The modified blade experiences a noticeable reduction in power output, with a 20% decrease in the power coefficient (Cp = 0.2 compared to Cp = 0.25 for the baseline design). Although the leading-edge tubercles enhance the power coefficient within a narrow range of blade positions (e.g., at 75°), this improvement is offset by a significant reduction in aerodynamic performance at other angular positions. Consequently, the overall power coefficient of the turbine exhibits greater fluctuations and a lower average value. Regarding the forces acting on the rotor, the modification results in an increase in the azimuthal force.

This reduction in turbine performance can be explained by analyzing the lift and drag coefficients of a single blade. The sinusoidal leading edge demonstrates improved performance over a range of blade positions between 0° and 100°, but this trend shifts around 200°, where the baseline blade shows superior lift and similar drag forces. The airfoil thus exhibits better aerodynamic performance up to the leeward position, but its performance declines significantly after profile separation occurs. It is, however, important to note that the effects of varying the amplitude and wavelength combinations, as well as the adoption of a double sinusoidal profile, still require investigation. These modifications could potentially mitigate the performance loss observed at certain blade angles.

7 ACKNOWLEDGEMENTS

The authors acknowledge the Ministry of University and Research (MUR) as part of the PNRR, Spoke 6 “Multiscale Modelling and Engineering Application” in CN1-HPC “National Center on HPC, Big Data and Quantum Computing” and PNRR - M4C2 - PE0000021 ”NEST – Network 4 Energy Sustainable Transition” in Spoke 2 ”Energy Harvesting and Off-shore renewables”.

Nomenclature

δ	boundary layer thickness [mm]
θ	blade position [mm]
c	blade chord [m]
D	turbine diameter [m]
TSR	tip-speed ratio [-]
Cp	power coefficient [-]
Cd	drag coefficient (single blade) [-]
Cl	drag coefficient (single blade) [-]

References

[1] Costanzo, G., Brindley, G., & Cole, P. (2023). Wind energy in Europe - 2022 Statistics and the outlook for 2023-2027. Wind Europe.

[2] Battisti, L. (2011). Gli impianti motore eolici. Trento: Green Place Energies.

[3] Dominy, R., Lunt, P., & Dominy, J. (2006). Self-starting capability of a Derrieus turbine. IMechE, 221.

[4] Mostafa, W., Abdelsamie, A., Sedrak, M., Thevenin, D., & Mohamed, M. (2021). Quantitative impact of a micro-cylinder as a passive flow control on a vertical axis wind turbine performance. Elsevier.

[5] Zhu, H., Hai, W., Li, C., & Ding, Q. (2019). A critical study on PFC techniques for straight bladed vertical axis wind turbines. Elsevier.

[6] Zamani, M., Nazari, S., Moshizi, S., & Maghrebi, M. (2016). Three dimensional simulation of J-shaped Darrieus vertical axis wind turbine. Elsevier.

[7] Wang, Y., Sun, X., Dong, X., Bing, Z., & Zheng, Z. (2015). Numerical investigation on aerodynamic performance of a novel vertical axis wind turbine with adaptive blades. Elsevier.

[8] Corsini, A., Delibra, G., & Sherard, A. (2013). On the role of leading-edge bumps in the control of stall onset in axial fan blades. Journal of fluids engineering.

[9] Tieghi L., D. G. (2024). Design of Sinusoidal Leading Edge for Low-Speed Axial Fans Operating under Inflow Distortion. Energies, 17(5).

[10] Wang, Z., & Zhuang, M. (2017). Leading-edge serrations for performance improvement on a vertical-axis wind turbine at low tip-speed-ratios. Elsevier.

[11] Wei, Z., New, T., & Cui, Y. (2015). An experimental study on flow separation control of hydrofoils with leading-edge tubercles at low Reynolds number. Elsevier.

[12] Johari, H., Henoch, C., Custodio, D., & Levishin, A. (2007). Effects of Leading-Edge Protuberances on Airfoil Performance. AIAA.

[13] Lin, S., Lin, Y., Bai, C., & Wang, W. (2015). Performance analysis of vertical-axis-wind-turbine blade with modified trailing edge through computational fluid dynamics. Elsevier.

[14] Longhuan Du, R. G. (2021). Experimental Investigation of the Performance of H-Darrieus Wind Turbines With Tubercle Leading Edge Blades . Proceedings to ASME Turbo Expo 2020: Turbomachinery Technical Conference and Exposition.

[15] Chang, H. L. (2024). Effect of discontinuous biomimetic leading-edge protuberances on the performance of vertical axis wind turbines. Applied Energy.

[16] Bravo, R. T. (2007). Performance testing of a small vertical-axis wind turbine. Proceedings of the 21st Canadian Congress of Applied Mechanics, 3-7.